

Headline Articles

In Situ Time-Resolved Energy-Dispersive XAFS Study on the Reduction Processes of Cu–ZSM-5 Catalysts

Aritomo Yamaguchi, Takafumi Shido, Yasuhiro Inada,† Toshihiro Kogure,†† Kiyotaka Asakura,††† Masaharu Nomura,†††† and Yasuhiro Iwasawa*

Department of Chemistry, Graduate School of Science, the University of Tokyo, Hongo, Bunkyo-ku, Tokyo 113-0033

†Research Center for Materials Science, Nagoya University, Nagoya 464-8602

††Department of Earth and Planetary Science, Graduate School of Science, the University of Tokyo, Hongo, Bunnkyo-ku, Tokyo 113-0033

†††Catalysis Research Center, Hokkaido University, Kita-ku, Sapporo 060-0811

††††Institute of Materials Structure Science, Photon Factory, KEK, Ibaraki 305-0801

(Received November 10, 2000)

The reduction process of Cu–ZSM-5 was investigated by a time-resolved energy-dispersive XAFS (DXAFS) technique. The spectra were recorded every second and the entire spectra were analyzed to elucidate the dynamic change of the local structure around the Cu species. Two Cu–ZSM-5 samples with different Cu loadings were prepared by an ion-exchange method followed by calcination. In the low-loading sample (84% ion-exchanged), Cu^{2+} cations dispersed isolatedly in the channels of ZSM-5, while in the high-loading sample (104% ion-exchanged) CuO particles were formed. The isolated Cu^{2+} cations were reduced to isolated Cu^{2+} cations at 400–450 K and the Cu^{+} ions were reduced to Cu^{0} at 550–650 K. The curve fitting analysis of the DXAFS data revealed that Cu_{4-6} clusters were initially formed in the reduction process. The clusters went out to the outer surface and grew into big particles. On the contrary, the CuO particles on the outer surfaces were reduced directly to Cu^{0} metallic particles at ca. 450 K. The dynamic structure change around the Cu species in the zeolite during the reduction with H_2 was monitored in situ by DXAFS technique for the first time.

Elucidating the dynamic structure change of catalyst precursors during the chemical treatments is a key issue to understand the chemistry of catalyst preparation and activation processes and to develop efficient catalytic materials. Reduction of catalyst precursors is often used to activate catalysts and the property of the precursors during reduction has been characterized by temperature-programmed experiments which monitor desorbed species, consumption of gases, or catalyst weight. However, these techniques give little information on the structure of catalyst precursors in the reduction process. Thus the structure and dynamic behavior of catalyst precursors in the catalyst preparation should be investigated in situ by means of time-resolved spectroscopies.

X-ray absorption fine structure (XAFS) has been used to explore the structure of noncrystalline materials such as catalysts and catalyst precursors.[1,2] This technique suits investigating dynamic structure changes during catalyst pretreatments because the XAFS spectra can be recorded in gas atmospheres. The duration of data acquisition in a conventional XAFS technique, however, is more than 10 min, and the applications to exploitation of dynamic processes has been limited to very slow systems.

Recently, time-resolved (TR) XAFS has been developed and changing structures can be investigated using the TR-XAFS. There are two methods for TR-XAFS: one is quick XAFS (QXAFS)[3,4] and the other is energy-dispersive XAFS (DXAFS)[5]. There are several advantages and disadvantages in these two techniques. A crucial advantage of the DXAFS technique over the QXAFS technique is that all the data points in a spectrum are simultaneously measured in the DXAFS technique.

In this study we have studied the reduction process of Cu–ZSM-5 catalysts during temperature-programmed reduction (TPR) by DXAFS. Cu–ZSM-5 has a unique catalytic property for NO decomposition.[6–10] Isolated Cu^{2+} ions, $[Cu–O–Cu]^{2+}$ oxocations and CuO particles have been identified in calcined Cu–ZSM-5 samples.[11,12] The redox properties of Cu in Cu–ZSM-5 are assumed to be essential for NO decomposition. However, the structural change of the Cu species that occurs during the reduction with H_2 is still unknown. We prepared

two Cu–ZSM-5 samples having isolated Cu^{2+} species in the channels of ZSM-5 and CuO particles on the outer surfaces of ZSM-5 to examine how the initial state of Cu species affects the reduction process.

Experimental

Sample Preparation. The Cu–ZSM-5 samples were prepared by an ion exchange method using copper nitrate solution. A given amount of an aqueous solution of copper(II) nitrate trihydrate $Cu(NO_3)_2 \cdot H_2O$ (Wako 99.9%) (0.1 mol dm^{-3}) was used to ion-exchange the proton of HZSM-5 (Tosoh HSZ-820NAA, SiO_2/Al_2O_3 = 23.8). The pH during the ion exchange was 5.5. After continuous stirring for 24 h at room temperature, the sample was filtered and then washed by distilled water several times, and then dried at 393 K for 6 h. The obtained sample was calcined in a flow of O_2 (20%)/He (80%) (50 cm^3 min^{-1}) at 773 K for 2 h before reduction. The Cu amount in ZSM-5 was determined by X-ray fluorescence (XRF) technique (SEIKO SEA-2010). The degree (%) of the ion exchange was defined as Cu/Al×200 and determined to be 84%. This sample is denoted as Cu–ZSM-5-A hereinafter. The sample with 104% ion exchange (denoted as Cu–ZSM-5-B) was prepared under the condition where the pH of the suspension during ion exchange was increased to 7 by addition of diluted aqueous ammonia solution. The samples were reduced in the temperature-programmed reduction (TPR) condition at a heating rate of 5 K min^{-1} and a H_2 pressure of 5.3 kPa *in situ* in a DXAFS cell. Transmission electron microscope (TEM) images were measured using a Hitachi HF-2000 electron microscope with a cold field-emission gun operated at 200 kV.

DXAFS Measurements. Energy-dispersive XAFS measurements were carried out using synchrotron radiation at BL-9C at KEK-PF in Institute of Materials Structure Science. The ring energy and current were 2.5 GeV and 200–350 mA, respectively. A triangle-shaped Si(111) bent crystal was used to focus polychromatic X-ray beams. The length and width of the crystal were 200 and 85 mm, respectively. The crystal was bent with a radius of curvature of 3700 mm. The distance between the crystal and the focus was approximately 400 mm and the horizontal width of the focus was about 0.8 mm. The sample was placed at the focus. A Pt-coated mirror was placed behind the sample to reject higher-order harmonics. The diverging X-rays were detected by a position-sensitive X-ray detector, a photodiode array manufactured by HAMAMATSU Photonics. The detector consisted of 1024 sensing elements (0.025 mm wide, 2.5 mm high) and a fluorescence material coated fiber-plate in front of the sensing elements. The energy resolution was 3–5 eV. Energy calibration was carried out by using a spectrum for Cu foil. The channels of the photodiode array were correlated to the X-ray energy with a second-order polynomial. The energy range was 8800–9800 eV. The sample was mounted in a stainless-steal cell with two Kapton windows and an electro-magnetic valve. The valve can be operated from the outside of the hutch and the sample can be evacuated and exposed to H_2 gas during the measurements. The cell was placed at such a position that the sample was located at the focusing point. A slit with 1 mm width was set just before the sample to block stray light. The sample thickness was regulated so that the edge jump was ca. 1.0. The X-ray absorption spectra were calculated by $\ln(I_0(E)/I(E))$, where $I(E)$ and $I_0(E)$ are X-ray intensity with and without sample as a function of X-ray energy (E). The measuring conditions for I and I_0 were controlled to be as equal as possible, except for the sample mounting, to avoid making artifacts. The spectra were acquired at intervals of 1 s under the TPR condition and analyzed by the UWXAFS package.[13] After background subtraction, k^3-weighted EXAFS functions were Fourier-transformed into a R-space and fitted in the R-space. The k range of the Fourier transformation and the fitting R range were 30–90 nm^{-1} and 0.08–0.3 nm, respectively. The spectra were fitted by three shells at most: Cu–O, Cu–Cu and Cu–(O)–Cu. The back-scattering amplitudes and phase shifts were calculated by the FEFF8 code.[14] The reported values of the coefficients of effective amplitude reduction factor were used in the fittings: 0.80 for Cu–O, and 0.92 for Cu–Cu and Cu–(O)–Cu.[15] The fitting parameters were a coordination number (CN) and an interatomic distance (R) for each shell, and a correction of the threshold energy (ΔE_0). The calculated Debye–Waller factors were used to fit the DXAFS spectra. They were calculated from Debye temperatures (Θ_D) and the temperature-independent part of the Debye–Waller factor (σ_0) obtained from conventional EXAFS spectra measured at different temperatures for Cu–ZSM-5-A and Cu–ZSM-5-B before and after the reduction and a reduced Cu–ZSM-5-A at 500 K. Different ΔE_0's were used for metallic Cu and Cu cations (Cu^+ and Cu^{2+}). They were fixed at certain values and the same values were used in the same series of DXAFS spectra. The values were determined so that the average residual factor became a minimum. As a consequence, the number of fitted parameters was at most six (CN and R for Cu–Cu, Cu–O and Cu–(O)–Cu), which is smaller than the number of the independent parameters calculated from the Niquest law[16] (eight, in this case).

Conventional XAFS spectra were measured at BL-10B at KEK-PF in Institute of Materials Structure Science at several temperatures to estimate the Debye–Waller factors. The measuring conditions are described elsewhere.[17]

Results

TEM Observation. Figures 1a–d show TEM photographs of Cu–ZSM-5-A and Cu–ZSM-5-B before and after reduction with H_2, respectively. The TEM photograph of Fig. 1c for the calcined Cu–ZSM-5-B sample showed that CuO particles (indicated by arrows) were formed on the outer surfaces of ZSM-5, while the copper species in the calcined Cu–ZSM-5-A sample were suggested to be highly dispersed in the ZSM-5 channels, as shown in Fig. 1a. After the TPR, large Cu particles (10–20 nm) were observed in both Cu–ZSM-5-A and Cu–ZSM-5-B. The contrasted images in Figs. 1b–d were characterized by electron diffraction patterns.

XANES Analysis. Figures 2a and b show the series of X-ray absorption spectra (XAS) of Cu–ZSM-5-A (a) and Cu–ZSM-5-B (b), respectively. As the edge shape is affected by the oxidation state of Cu species, the proportion of Cu^{2+}, Cu^+, and Cu^0 species can be estimated by linear least-square fitting if the X-ray absorption near edge structure (XANES) spectra (X) were represented by a linear combination of reference spectra (Y_i).

$$X = \sum_i c_i Y_i. \tag{1}$$

where c_i is the coefficient of i-th contribution.

Figures 3a–c show the results of the XANES analysis. The fitting energy range was 8950–9050 eV. When the XANES spectra of Cu–ZSM-5-A was fitted by a linear combination of the spectra at 300 and 700 K, the XANES spectra in the tem-

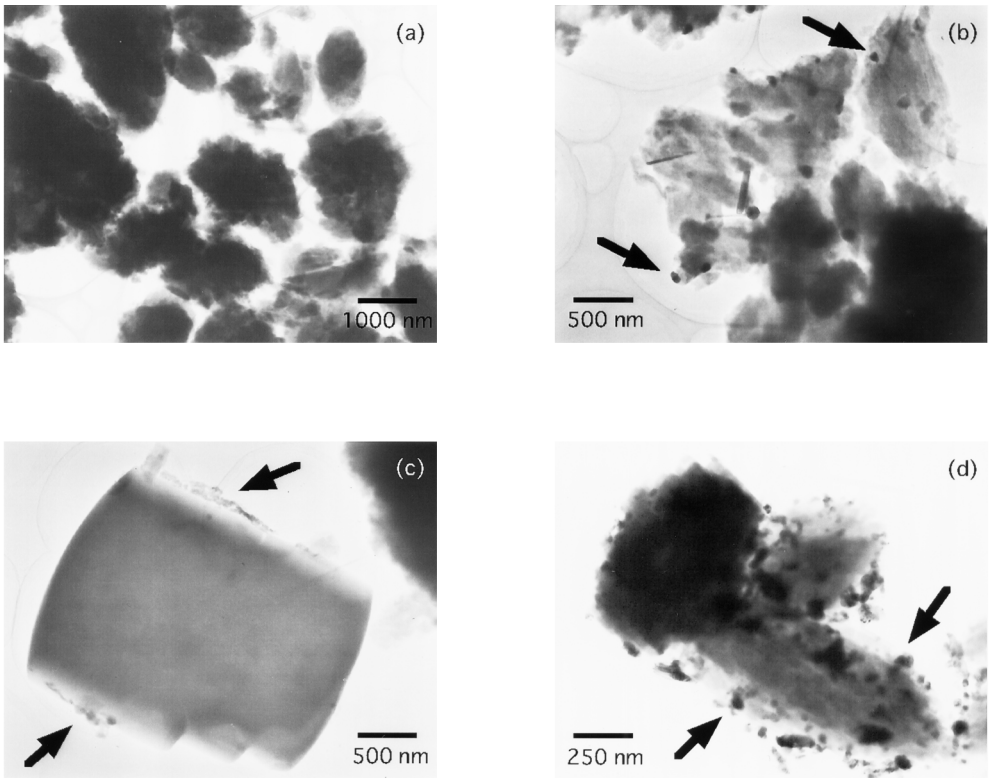

Fig. 1. TEM images of Cu–ZSM-5-A before (a) and after (b) TPR, and those of Cu–ZSM-5-B before (c) and after (d) TPR. Arrows indicate Cu or CuO particles on the outer surfaces of ZSM-5.

perature range 450–550 K cannot be fitted properly as suggested by large residual factors ($R_f > 5\%$). The results are shown in Fig. 3a. Thus the spectra were fitted by three references: the spectra measured at 300, 500, and 700 K, as shown in Fig. 3b. The XANES spectra at 300, 500, and 700 K which were used as references for the fitting of XANES spectra may be the ones for Cu^{2+}, Cu^{+}, and Cu^{0} species as explained in Discussion section 4.2.

The coefficient for "Cu^{2+}" decreased at 400–450 K accompanied with an increase of that for "Cu^{+}", and the coefficient for "Cu^{+}" decreased at 550–620 K accompanied with an increase of that for "Cu^{0}". The sum of the coefficients was very close to unity and the R_f was less than 0.6% over the whole temperature range. The results of the XANES analysis showed that the reduction of Cu^{2+} cations in Cu–ZSM-5-A proceeded by two successive steps and that the Cu species present at 400–600 K was not a mixture of "Cu^{2+}" and "Cu^{0}".

On the contrary, the XANES spectra for Cu–ZSM-5-B can be reproduced by the two reference spectra for "Cu^{2+}" and "Cu^{0}" species. The sum of the coefficients was close to unity and the R_f was less than 2.0%, as shown in Fig. 3c. The coefficient for "Cu^{2+}" began to decrease at 400 K, accompanied with an increase of that for "Cu^{0}" species.

Hydrogen uptakes in the TPR profiles for Cu–ZSM-5-A and Cu–ZSM-5-B were observed at similar temperatures to those where the coefficients changed, as shown in Fig. 3. The agreement between the XANES analysis and the TPR profiles suggest that the changes in the coefficients are due to the reduction of the copper species in the ZSM-5 zeolites.

Curve Fitting of EXAFS. Figure 4a shows a typical k^3-weighted EXAFS function for a calcined Cu–ZSM-5-A obtained by the DXAFS measurement. The quality of the spectrum was reasonably good for the curve fitting analysis up to $k = 90$ nm^{-1}. Figure 4b shows the Fourier-transformed k^3-weighted EXAFS function (FT($k^3\chi(k)$)) obtained from the spectrum shown in Fig. 4a, together with the result of curve fitting. The k range for the Fourer transformation was 30 nm$^{-1} \leq k \leq 90$ nm^{-1}. No phase shift correction was carried out in Fig. 4b.

Figures 5a and b show the absolute values in FT($k^3\chi(k)$) for Cu–ZSM-5-A (a) and Cu–ZSM-5-B (b) as a function of reduction temperature (phase shift uncorrected). In Fig. 5a, a large peak of Cu–O bonding was observed at 0.15 nm at 300 K. The peak height decreased to be half at 400–450 K without changing the peak position. The peak of Cu–O decreased further above 550 K and a new peak of Cu–Cu appeared at 0.20 nm and grew with increasing temperature. The results also suggest that the reduction of Cu^{2+} species in Cu–ZSM-5-A proceeds through two steps.

In Fig. 5b, two peaks for Cu–O and Cu–(O)–Cu bondings were observed at 0.15 and 0.25 nm at 300 K. These peaks disappeared and a peak for metallic Cu–Cu bonding appeared at 0.20 nm at 450–500 K. The results suggest that the Cu^{2+} species in Cu–ZSM-5-B were reduced directly to Cu^{0} species.

In order to obtain detailed information about the structural transformation of the Cu species, the curve fitting analysis for the DXAFS data was carried out. The Fourier-transformed EXAFS functions were fitted to elucidate the structural parameters around Cu species. Figures 6a–f show R, CN, and R_f against reduction temperature for Cu–ZSM-5-A and Cu–ZSM-

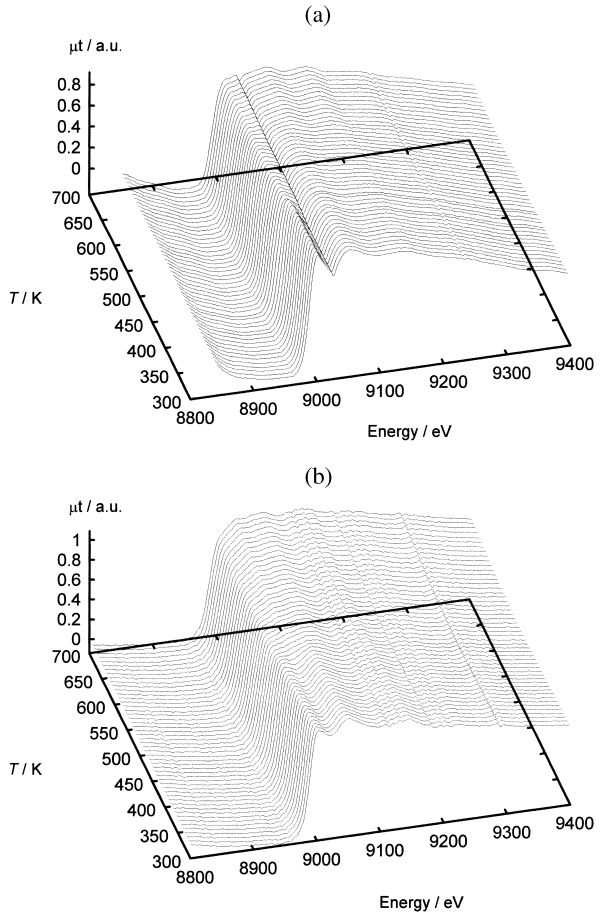

Fig. 2. Energy dispersive X-ray absorption spectra at Cu K-edge for (a) Cu–ZSM-5-A and (b) Cu–ZSM-5-B during the TPR under 5.3 kPa of H_2 from 300 to 700 K at a heating rate of 5 K min^{-1}. The acquisition time of each spectrum is 1 s.

5-B. For both Cu–ZSM-5-A and Cu–ZSM-5-B, the Cu–O and metallic Cu–Cu distances were calculated to be 0.195 ± 0.003 and 0.251 ± 0.003 nm, respectively. In addition to these bondings, the Cu–(O)–Cu distance was calculated to be 0.293 ± 0.003 nm in the Cu–ZSM-5-B. The interatomic distances did not change with reduction temperature within the error bars in both Cu–ZSM-5-A and Cu–ZSM-5-B, as shown in Figs. 6b and e.

The CN values varied with reduction temperature, on the other hand. As shown in Fig. 6a, the CN of Cu–O in Cu–ZSM-5-A decreased in two stages. It was ca. 2.8 in the temperature range 300–400 K and began to decrease at 400–450 K and became constant at ca. 1.4 in the temperature range 450–550 K. The CN of Cu–O began to decrease again above 550 K and became almost zero above 650 K. The Cu–Cu bonding appeared at 550 K and the CN of Cu–Cu increased with increasing temperature. It reached 7.8 at 700 K.

For Cu–ZSM-5-B, the CN's for Cu–O and Cu–(O)–Cu at 300 K were calculated to be 3.8 and 2.5, respectively. They began to decrease above 430 K. The Cu–O and Cu–(O)–Cu bonds were observed up to 700 K, which implies that a part of CuO particles remain unreduced even at 700 K.

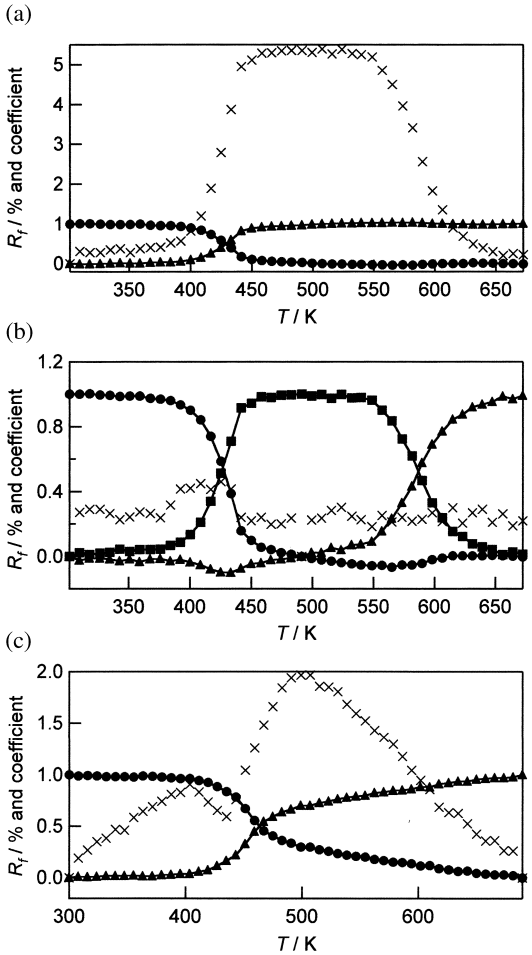

Fig. 3. The proportion of Cu^0 (c_0, ▲), Cu^+ (c_1, ■), and $Cu2^+$ (c_2, ●) against reduction temperature delivered by linear least square fitting of the XANES spectra, as well as *R* factors (%) (×). (a) The results of the XANES analysis for Cu–ZSM-5-A fitted by the linear combination of two references; the spectra measured at 300 K (reference for Cu^{2+}) and a 700 K (reference for Cu^0). (b) The results of the XANES analysis for Cu–ZSM-5-A fitted by the linear combination of three references; the spectra measured at 300 K (reference for Cu^{2+}) at 500 K (reference for Cu^+) and at 700 K (reference for Cu^0). (c) The results of the XANES analysis for Cu–ZSM-5-B fitted by the linear combination of two references; the spectra measured at 300 K (reference for Cu^{2+}) and at 700 K (reference for Cu^0).

Discussion

EXAFS Analysis. As the *k* range of the DXAFS spectra was limited (Δk = 60 nm^{-1} in this study), the number of free parameters for the fitting analysis should be reduced. The strategy in this paper is to use the Debye–Waller factors calculated from the EXAFS spectra for Cu^0, Cu^+, and Cu^{2+} species in Cu–ZSM-5-A and Cu–ZSM-5-B at several temperatures by using a conventional XAFS technique. The Debye temperature (Θ_D) and the temperature independent part of the Debye–Waller factor (σ_0) can be calculated from the EXAFS spectra measured at several temperatures. As the *k* range of the con-

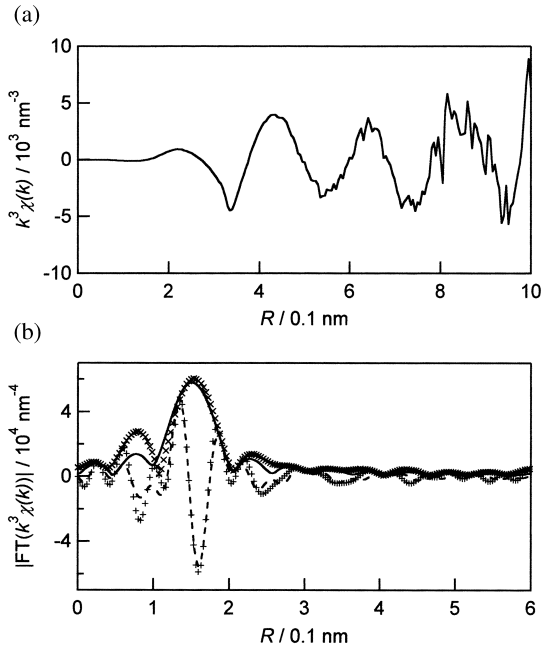

Fig. 4. (a) A typical k^3-weighted EXAFS function for Cu–ZSM-5-A during TPR measured by DXAFS. The EXAFS spectrum was measured at 300 K and the data acquisition time was 1 s. (b) Fourier transformation of the spectrum (a) and its curve fitting result; (×××) absolute values of observed data, (+++) imaginary part of observed data, (solid line) absolute values of calculated spectrum, (broken line) imagninary part of calculated spectra.

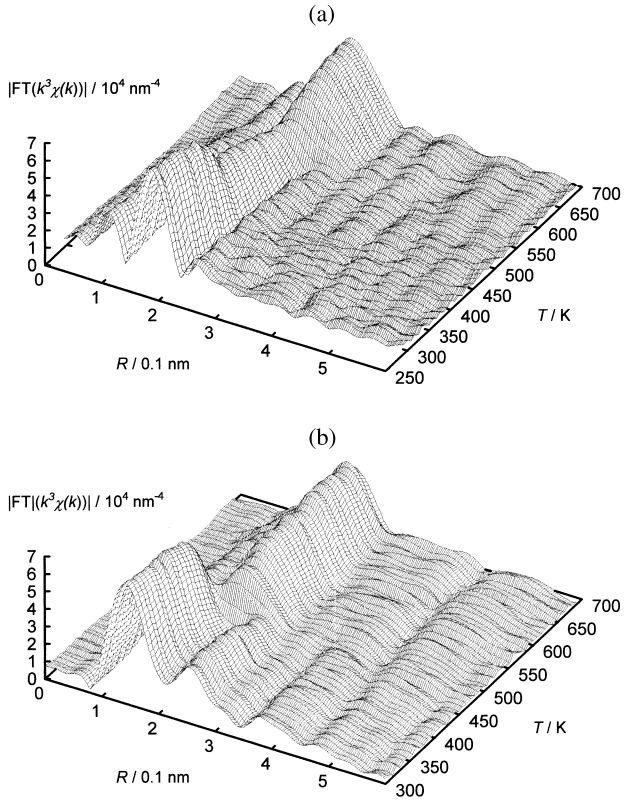

Fig. 5. A series of Fourier transformed k^3-weighted EXAFS function against reduction temperature. (a) Cu–ZSM-5-A and (b) Cu–ZSM-5-B.

ventional EXAFS spectra was wide (30 nm^{-1} ≤ k ≤ 150 nm^{-1} in this study), these parameters can be calculated accurately. The Debye–Waller factor (σ) at a temperature T can be calculated as a sum of the σ_0 and the temperature depending part of Debye–Waller factor (σ_T), which can be calculated from Θ_D and T,[18]

$$\sigma^2 = \sigma_T^2(T, \Theta_D) + \sigma_0^2 \quad (2)$$

As the Θ_D for Cu–Cu (322 K) is lower than the measuring temperature, the unharmonic distribution in the Cu–Cu bond length may cause the underestimation of the CN for metallic Cu–Cu. Clausen et al. studied the effect of Cu particle size and measuring temperature using molecular dynamic simulation and found that the CN for Cu–Cu is underestimated substantially when the EXAFS spectra are measured at higher temperatures (say 587 K, which is the temperature they investigated) and analyzed by a conventional curve fitting with free CN, R, and Debye–Waller factor.[19,20] The magnitude of the underestimation becomes larger when the particle size becomes smaller. Thus the CN's for Cu–Cu obtained by the DXAFS curve fitting analysis could be somehow smaller than the real values.

XANES Analysis. The number of Cu species and their proportion can be estimated by XANES analysis. The series of XANES spectra were reproduced by the linear combination of reference spectra. The XANES spectra before and after reduction were taken as reference; observed XANES spectra during TPR were expressed as the linear combination of these two spectra. In the case of Cu–ZSM-5-B, the XANES spectra during TPR can be reproduced well by a linear combination of the reference spectra before and after reduction. On the other hand, the XANES spectra during the TPR of Cu–ZSM-5-A cannot be reproduced well by a linear combination of these two spectra measured before and after reduction. Especially, the spectra between 450–550 K cannot be reproduced, as shown in Fig. 3a. The result suggests that intermediate Cu species exist in this temperature range and another reference spectrum is required to fit the XANES spectra. When the spectrum measured at 500 K was used as a third reference, the series of XANES spectra were fitted well, as shown in Fig. 3b. However, the coefficients for Cu^0 and Cu^{2+} were slightly negative in the 400–450 and 550–600 K ranges, respectively. These temperature ranges correspond to transient states of Cu species. The negative coefficients for Cu^0 and Cu^{2+} might be due to analysis error and/or unstable species might exist during the transformation. In the case of DXAFS measurements, the analysis error might be large as compared to conventional XAFS measurements because the three reference spectra were not completely independent, due to not so good energy resolution (3–5 eV). However, the deviation of the coefficients in these temperature ranges is small and insignificant. Hence, we neglect them in this study.

As the XANES spectra are affected by the local structure as well as by the oxidation state of the metal, the species with similar structures should be used as references. The XANES spectra for the Cu–ZSM-5 samples could not be reproduced by the linear combination of the XANES spectra for bulk CuO,

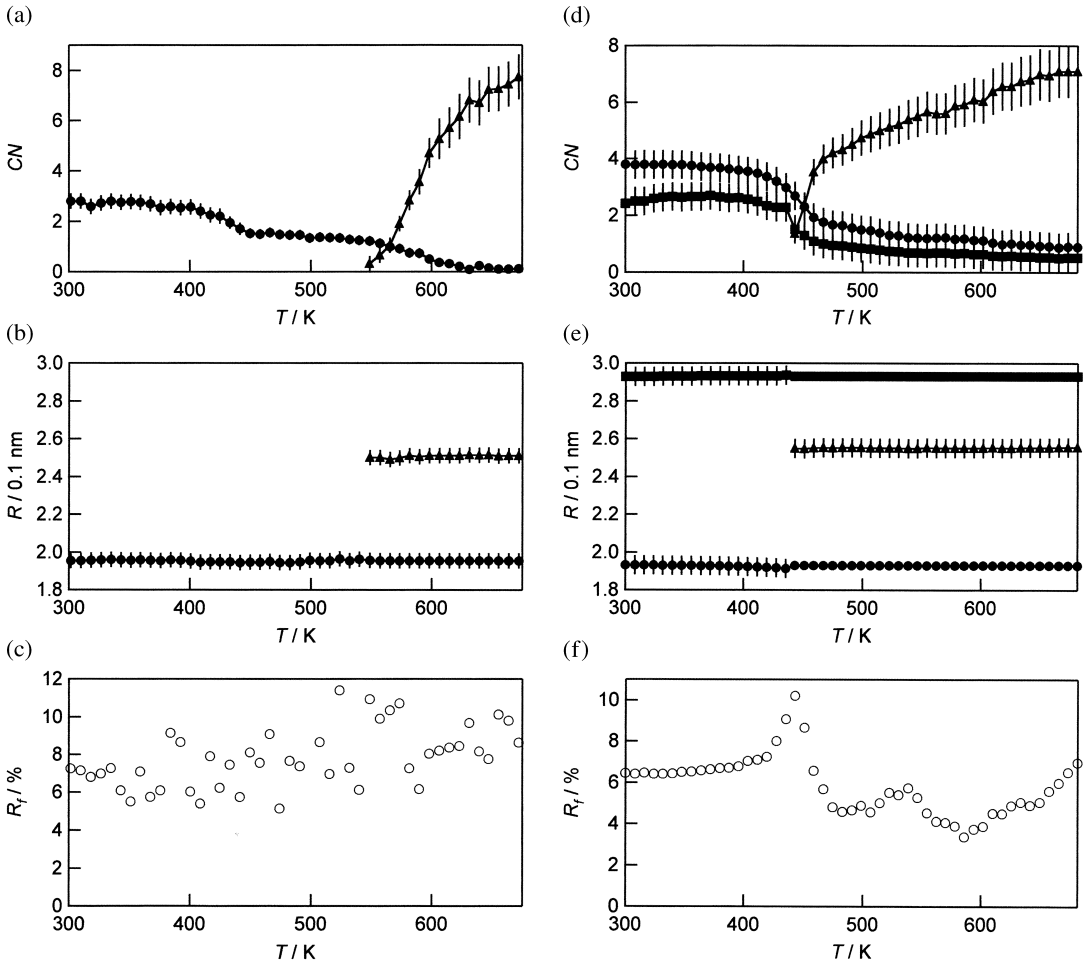

Fig. 6. Structural parameters for Cu–ZSM-5-A and Cu–ZSM-5-B delivered by the curve fitting analysis of the DXAFS data for Cu–ZSM-5-A (a–c) and Cu–ZSM-5-B (d–f) against reduction temperatures; (●) Cu–O, (▲) metallic Cu–Cu, (■) Cu–(O)–Cu.

Cu_2O, and Cu foil. In this study, accordingly, the XANES spectra for the Cu–ZSM-5 samples measured at 300 and 700 K were regarded as references for Cu^{2+} and Cu^0 species. In addition to this, the spectrum measured at 500 K was used as a reference for Cu^+ in the case of Cu–ZSM-5-A. If the reference spectra represent "pure" Cu^0, Cu^+, or Cu^{2+} species, the coefficients obtained by the XANES analysis indicate the proportion of these Cu species. Even if the reference spectra are mixtures, however, the proportion of Cu^0, Cu^+, and Cu^{2+} species can be calculated easily if the reference spectra Y_i in (Eq. 1) is a linear combination of the spectra of "pure" Cu^0, Cu^+, or Cu^{2+} species (R_j):

$$Y_i = \sum_j x_{ij} R_j. \tag{3}$$

In this case, the proportion of the j-th species p_j in the sample can be calculated as

$$P_j = \sum_i c_i x_{ij} \tag{4}$$

As a result, if the proportions of Cu^0, Cu^+, and Cu^{2+} species in the reference are known, the proportion of the Cu species during the reduction can be estimated.

It should be reasonable to assume that the calcined sample before the reduction contains only Cu^{2+} species. On the other hand, it is not always guaranteed that all the Cu species are reduced to Cu^0 species and the proportion of the reduced Cu species after reduction should be estimated. In the case of the Cu–ZSM-5-A sample, as the CN for Cu–O became zero above 640 K, it is evident that all the Cu species were reduced to Cu^0 at 700 K. In the case of the Cu–ZSM-5-B sample, on the contrary, Cu–O and Cu–(O)–Cu bonds were observed at 700 K, with the CN's of 0.9 ± 0.4 and 0.6 ± 0.4, respectively, which means that a part of the Cu species remained unreduced. This is probably because the inside of the big CuO particles at the outer surfaces of ZSM-5 was not reduced by the TPR condition. Thus, the local structure of Cu^{2+} species inside the big CuO particles remained unchanged during the reduction, while the surface layers of the particles were reduced to the metallic state. The decrease of the CN can be attributed to the decrease in the proportion of Cu^{2+} species. As a result, the proportion of Cu^{2+} was estimated to be 27% from the CN, and so 73% of the Cu species were reduced to Cu^0 at 700 K.

The XANES spectra for Cu–ZSM-5-A at 500 K was used as a reference for Cu^+ species. As the metallic Cu–Cu bonds were not observed at 500 K, Cu^0 species did not exist in the

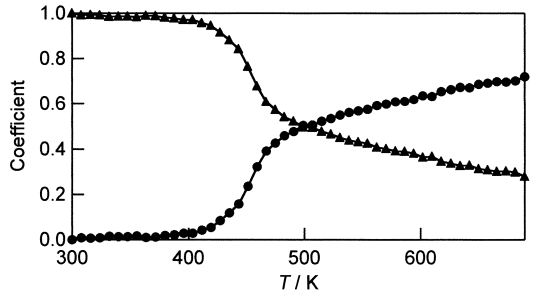

Fig. 7. Proportion of Cu^{2+} (▲) and Cu^0 (●) species in Cu–ZSM-5-B against reduction temperature. The proportion was estimated by taking the ratio of Cu^{2+} species in the spectrum measured at 700 K, which was used as a reference spectrum for Cu^0 species in Cu–ZSM-5-B in Fig. 3.

sample at this stage. As two peaks for H_2 consumption at 460 and 600 K in the TPR profile were clearly separated, the amount of Cu^{2+} seems to be fractional in the Cu–ZSM-5-A sample reduced at 500K. In addition, the coefficient for Cu^+ was unity over a wide temperature range. Thus, we assume that the XANES at 500 K represents only Cu^+ species. The structural parameters for isolated Cu species in Cu–ZSM-5-A derived from the EXAFS analysis agree with the parameters in the previous study.[21]

From these discussions, we conclude that the coefficients delivered by the XANES analysis for the Cu–ZSM-5-A sample represent the proportion of Cu^0, Cu^+, and Cu^{2+} species. On the contrary, as the Cu–ZSM-5-B samples after the reduction at 700 K is a mixture of Cu^0 (73%) and Cu^{2+} (27%) species, the proportion of Cu species during TPR should be calculated by taking the proportions of Cu^0 and Cu^{2+} at 700 K into account. Figure 7 shows the proportions of Cu^0 and Cu^{2+} species in Cu–ZSM-5-B as a function of reduction temperature by using Eqs. 3 and 4. It depicts that half of Cu^{2+} species were reduced to Cu^0 at 450–500 K and the reduction continued slowly up to 700 K.

Growth of Cu Metal Particles During the Reduction. Figure 8 shows the Cu–Cu coordination number of Cu metallic particles (CN(Cu–Cu)) as a function of reduction temperature. The CN(Cu–Cu) was calculated by dividing the observed CN for Cu–Cu by the proportion of Cu^0. The uncertainty was estimated from the uncertainty of the observed CN for Cu–Cu and the proportion of Cu^0 species. As shown in Fig. 8a, the CN(Cu–Cu) in Cu–ZSM-5-A increased with temperature from 3.4 ± 0.4 at 550 K to 7.8 ± 1.0 at 700 K. The results demonstrate clearly that particle growth occurred during the reduction. At the initial stage of the metallic Cu formation at 550 K, the CN(Cu–Cu) was 3.4 ± 0.4, which suggests that Cu_{4-6} small clusters were formed. The clusters are located in the channels of ZSM-5 zeolite because the diameter of Cu_{4-6} clusters is about 0.4 nm, which is smaller than the channel diameter of ZSM-5 (0.56 nm).

The CN(Cu–Cu) increased with temperature and reached 7.8 ± 1.0 at 700 K. This means that the average particle size increased with temperature. As only clusters smaller than the channel dimensions can exist in the channel, Cu clusters should go to the outer surfaces to form big Cu metallic particles. Thus the Cu^0 species in ZSM-5-A is a mixture of small

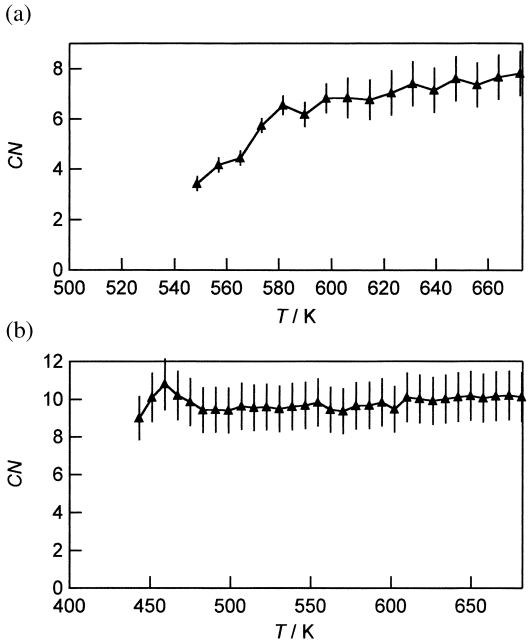

Fig. 8. Coordination number for metallic Cu–Cu bonds normalized by the proportion of Cu^0 as a function of reduction temperature. (a) Cu–ZSM-5-A, (b) Cu–ZSM-5-B.

clusters in the channel and big particles at the outer surfaces. This is supported by TEM in Fig. 1b which shows big Cu particles at the outer surfaces after the reduction at 700 K.

The particle size estimated from the CN(Cu–Cu) may be underestimated because of an unharmonic distribution of Cu–Cu interatomic distances at high temperatures.[19,20,22] In the present conditions, however, the effect is not so serious and the CN(Cu–Cu) is underestimated by 30% at maximum, which means that the size of the Cu particles is Cu_{6-13} at maximum. Even at the biggest case it is concluded that the Cu metallic particles are entrapped in the channels of ZSM-5.

In the case of the reduction of CuO big particles at the outer surfaces in Cu–ZSM-5-B, big Cu metallic particles were formed from the initial stage of the reduction at 440 K (the CN(Cu–Cu) at 440 K was 8.6 ± 1.0) and the CN(Cu–Cu) did not increase substantially with temperature, as shown in Fig. 8b. The Cu species were not reduced completely at 700 K because Cu–O and Cu–(O)–Cu bonds were observed at this temperature. This may be due to the experimental condition where the reduction was done by a sealed batch reactor with a relatively low hydrogen pressure of 5.3 kPa because of safety reasons at the synchrotron facility. Under the present reduction conditions, the big CuO particles are converted to egg-shell particles where only the Cu^{2+} species in the outer shell were reduced to the metallic state, while all the Cu^{2+} species in the ZSM-5 channels were reduced to metallic Cu particles as in the case of Cu–ZSM-5-A.

The Cu particle sizes estimated from the CN(Cu–Cu) and the TEM image for Cu–ZSM-5 are different from each other. The size from the CN(Cu–Cu) (1–3 nm) is much smaller than that from the TEM ($\geq$ 10 nm). The disagreement may be ascribed by the heterogeneous morphology and state of Cu particles. As a homogeneous spherical shape was assumed in esti-

mating the particle size from the CN, the particle size is underestimated if the particles are cored by unreduced species and only the surface is reduced.

Conclusions

Isolated Cu^{2+} species in the channels of ZSM-5 in the Cu–ZSM-5-A sample were reduced step by step: $Cu^{2+} \rightarrow Cu^{+} \rightarrow Cu^{0}$. The isolated Cu^{2+} ions were reduced to isolated Cu^{+} ions at 400–450 K and the Cu^{+} ions were reduced to Cu^{0} metallic species at 550–620 K. The reduction of Cu^{2+} to Cu^{+} proceeds faster than that of Cu^{+} to Cu^{0}. At the initial stage of the reduction of Cu^{+} ions, small Cu^{0} clusters were formed in the channels. At 700 K some of the clusters went out to the outer surfaces of the ZSM-5 to form Cu particles. On the contrary, big CuO particles on the outer surfaces in the Cu–ZSM-5-B sample were reduced directly to Cu^{0} big particles at 450 K. The CN of metallic Cu–Cu bonds and the TEM photograph showed that the Cu particles on the outer surfaces were big from the beginning and the particle growing process was not observed, unlike the case of Cu–ZSM-5-A. The temperature where the second reduction step $Cu^{+} \rightarrow Cu^{0}$ occurred was higher than the reduction temperature of the CuO particles to Cu^{0} particles. Probably the isolated Cu^{+} in the zeolite channel should migrate so as to gather each other for the reduction to metallic particles, while such a migration of Cu ions is not necessary in the CuO particles. We have succeeded in observing the time-resolved DXAFS spectra for Cu–ZSM-5 catalysts during the TPR process in 1 s time scale. It has been demonstrated that DXAFS is a powerful technique to characterize the dynamic behavior of metal sites dispersed in zeolites during reduction. The dynamic structural transformations of Cu species in ZSM-5, which cannot be obtained by other techniques, are elucidated by the DXAFS technique.

This work has been supported by CREST (Core Research for Evolutional Science and Technology) of Japan Science and Technology Corporation (JST). The XAFS measurements were done by the approval of the PAC committee (proposal No: 99G237).

References

1 "X-ray Absorption Fine Structure for Catalysts and Surfaces," ed by Y. Iwasawa, World Scientific, Singapore (1996).

2 "X-ray Absorption. Principles, Applications, Techniques of EXAFS, SEXAFS and XANES," ed by D. C. Koningsberger and R. Prins, Wiley, New York (1988).

3 R. Frahm, *Nucl. Instrum. and Meth. Phys. Res.*, **A270**, 578 (1988).

4 R. Frahm, *Rev. Sci. Instrum.*, **60**, 2515 (1989).

5 T. Matsushita and R. P. Phizackerley, *Jpn. J. Appl. Phys.*, **20**, 2223 (1981).

6 M. Iwamoto, H. Furukawa, Y. Mine, F. Uemura, S. Mikuriya, and S. Kagawa, *J. Chem. Soc., Chem. Commun.*, **1986**, 1272.

7 M. Iwamoto, H. Yahiro, K. Tanda, N. Mizuno, Y. Mine, and S. Kagawa, *J. Phys. Chem.*, **95**, 3727 (1991).

8 M. Iwamoto, H. Yahiro, N. Mizuno, W.-X. Zhang, Y. Mine, H. Furukawa, and S. Kagawa, *J. Phys. Chem.*, **96**, 9360 (1992).

9 M. Shelef, *Chem. Rev.*, **95**, 209 (1995).

10 V. I. Parvulescu, P. Grange, B. Delmon, *Catal. Today*, **46**, 233 (1998).

11 T. Beutel, J. Sarkany, G. D. Lei, J. Y. Yan, and W. M. H. Sachtler, *J. Phys. Chem.*, **100**, 845 (1996).

12 J. Sarkany, J. L. d'Itri, and W. M. H. Sachtler, *Catal. Lett.*, **16**, 241 (1992).

13 E. A. Stern, M. Newville, B. Ravel, Y. Yacoby, and D. Haskel, *Physica B*, **208**, 117 (1995).

14 A. L. Ankudinov, B. Ravel, J. J. Rehr, and S. D. Conradson, *Phys. Rev. B*, **58**, 7565 (1998).

15 G. G. Li, F. Bridges, and C. H. Booth, *Phys. Rev. B*, **52**, 6332 (1995).

16 E. A. Stern, *Phys. Rev. B*, **48**, 9825 (1993).

17 K. Asakura, Y. Noguchi, and Y. Iwasawa, *J. Phys. Chem. B*, **103**, 1051 (1999).

18 A. V. Poiarkova and J. J. Rehr, *Phys. Rev. B*, **59**, 948 (1999).

19 B. S. Clausen, L. Gråbæk, H. Topsøe, L. B. Hansenn, P. Stoltze, J. K. Nørskov, and O. H. Nielsen, *J. Catal.*, **141**, 368 (1993).

20 B. S. Clausen, J. K. Norskov, *Topics in Catal.*, **10**, 221 (2000).

21 H. Yamashita, M. Matsuoka, Y. Shioya, M. Anpo, and M. Che, *J. Phys. Chem.*, **100**, 397 (1996).

22 N. Van Hung, R. Frahm, and H. Kamitsubo, *J. Phys. Soc. Jpn.*, **65**, 3571 (1996).